Hindawi
Mathematical Problems in Engineering
Volume 2018, Article ID 4270790, 14 pages
https://doi.org/10.1155/2018/4270790

Research Article

Influence of Ignition Channel on the Ignition Performance of Ignition Device

Jiang Chang[1], **Gongping Wu**[1] **and Hanwei Tang**[2]

[1]*School of Power and Mechanical Engineering, Wuhan University, 299 Bayi Road, Wuhan, Hubei 430072, China*
[2]*The Fourth Research Academy, CASIC, 50 Beijing Road, Xiaogan, Hubei 432100, China*

Correspondence should be addressed to Gongping Wu; gpwu@whu.edu.cn

Received 13 December 2017; Revised 8 April 2018; Accepted 29 April 2018; Published 3 June 2018

Academic Editor: Marco Pizzarelli

Based on relative theories of gas dynamics and computational fluid dynamics, the flow field computation software ANSYS Fluent was used to simulate the steady flow field of the solid type ignition device of liquid-propellant rocket engine in two working conditions (condition I: without ignition channel, condition II: with ignition channel). On this basis, the influence of ignition channel on the working characteristics of the solid type ignition device of the liquid-propellant rocket engine was analyzed and experimentally tested. The results showed that when the pressure in the combustion chamber was atmospheric pressure, under condition II, the gas velocity at the throat of the ignition device did not reach the sonic velocity, and the position of sonic velocity moved to the downstream section of the ignition channel. Compared to condition I, the gas velocity and energy at the ignition outlet increased, which would be beneficial for initial ignition, and the gas pressure and temperature at the throat increased as well, indicating that the structural strength at the throat should be evaluated. The gas flow, gas pressure, and gas temperature at the ignition outlet decreased compared to working condition I, yet the changes were small and would have minimal effect on the ignition performance. During the pressure increase process in the combustion chamber, the gas pressure, velocity, temperature, flow, and energy at the ignition outlet experienced a steady stage in both working conditions before coming to an inflection point. The inflection point under condition II is smaller than that under condition I. To improve the ignition reliability, the working pressure of the ignition device should be further increased.

1. Introduction

For a solid type ignition device of a liquid-propellant rocket engine (hereinafter referred to as an ignition device), normal ignition of the engine is achieved by providing power to the igniter, which ignites the ignition powder and the main propellant grain in the ignition device, thereby producing high-temperature gas which is injected into the cavity of the main combustion chamber of the thrust chamber to ignite the propellant. As a key component of the liquid-propellant rocket engine, the ignition device's performance directly affects the normal operation of the liquid engine; thus it is very important to study the ignition performance of the ignition device.

There were numerous studies on the performance of ignition devices, which have effectively promoted the technological development of liquid-propellant engines. For example, Baudart conducted a numerical simulation of the ignition of the cryotechnic engine and that of the HM7B igniter in the main combustion chamber [1]. They study the complex transient reactive two phase flows. The effects related to liquid oxygen injection are highlighted. In a study by Buttay et al., the ignition process of the typical rocket engine igniter in the turbulent reaction flow was analyzed [2]. They study ignition processes in the turbulent reactive flow established downstream of highly under-expanded coflowing jets. Considering the discharge of axisymmetric coaxial under-expanded jets, various morphologies are expected, depending on the value of the nozzle pressure ratio, a key parameter used to classify them. The computational results reveal the complex topology of the compressible flow field. The obtained results also bring useful insights into the development of ignition processes. In particular, ignition is found to take place rather far downstream of the shock barrel, a conclusion

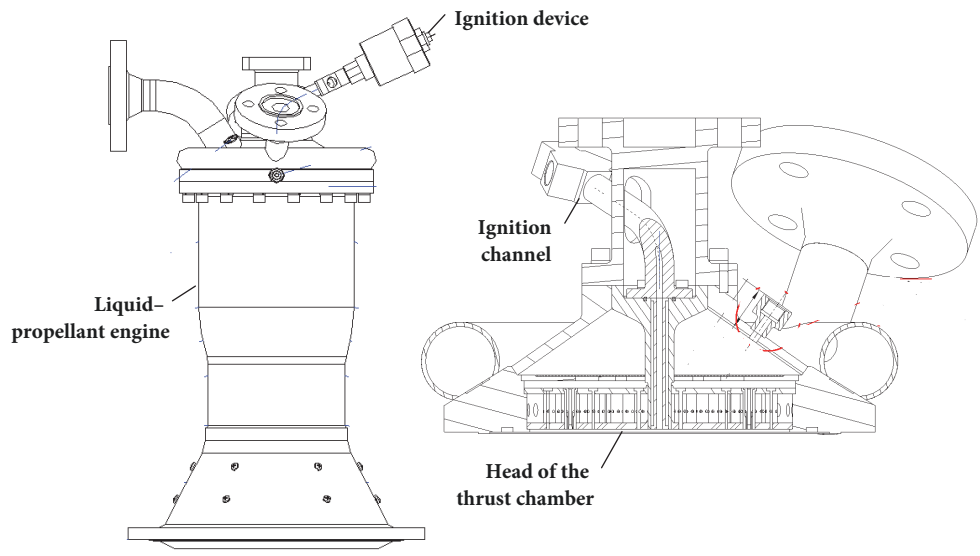

Figure 1: Installation of the ignition device in a liquid-propellant engine.

that contrasts with early computational studies conducted within the unsteady RANS computational framework. Popp et al. performed an experiment on the ignition moment of the HM7B igniter in the trust chamber [3]. Two separate test series were performed for the oxygen and the hydrogen flow circuits, respectively, to characterize the flow evolution before ignition. Important data were obtained providing knowledge of the transient filling of the LOX manifolds and the pre-cooling of the combustion chamber with hydrogen. Agostino et al. simulated the transient ignition process of the rocket engine [4]. Their study is detailing a simple model and the relative numerical solution method for the analysis of ignition transient. The model is capable of providing an accurate and reliable prediction of the most significant engineering quantities (pressure and velocity in the thrust chamber) for different rocket configurations. A theoretical quasi-one-dimensional model is derived from basic conservation laws, taking into account the initiation of combustion by the igniter discharge signal, the heat transfer from igniter combustion products to the propellant, the flame spreading flow field in the chamber, and the increase of chamber pressure up to the quasi-steady operating condition. The set of modeling equations are solved using a slightly modified Lax-Friedrichs method. In China, Chen et al. applied the CFD-ACE + flow field computation software to analyze the steady-state flow field of igniter working independently in the liquid combustor. How the ignition performance of the ignition device was influenced by the chamber pressure and structure of the igniter was analyzed on the basis of test validation. The analyzed result shows that, under the conditions of constant igniter temperature and gas flow rate, lower chamber pressure in igniter is more beneficial to ignition if expansion ratio remains unchanged [5]. In addition, in studies by Yang et al. and Tang et al., factors influencing the simulation of the flow field at the ignition moment of the rocket engine were explored, and a numerical simulation of the ignition process of the rocket engine was carried out [6–8]. The main influence factors of simulation, including the three cases of simplifying mode of igniter, selection mode of igniter output parameters, and firing mode, were analyzed. In order that the simulation results are well consistent with practical situation. Xu et al. analyzed the three-dimensional flow field of the ignition process of the rocket engine [9]. The changing trend of a shock wave in the nozzle during ignition start-up of SRM was calculated by using the finite volume method, which was consistent with the result of 1-D isentropic function theory. As shown in the results, the fuel gas behaves as subsonic flow in the combustion chamber and nozzle at the beginning of grain ignition.

The above studies have achieved remarkable results in analyzing the working performance of ignition devices, yet most of them are limited to analyses on the thermodynamic properties and working performance of ignition devices or liquid-propellant engine themselves. When an ignition device is installed on a liquid-propellant engine, the configuration is constrained by the structure of the liquid-propellant engine such that the high-temperature gas released from the ignition device usually needs to pass through a relatively long ignition channel before it is introduced into the main combustion chamber, which affects the ignition performance of the ignition device. Therefore, it is of great theoretical and engineering value to carry out a numerical simulation and experimental study on gas transmission in narrow channels. Little is known about the influences of the ignition channel on the ignition performance of ignition devices. Figure 1 shows the installation of the ignition device in a rocket engine. The ignition device is connected with the thrust chamber of the engine by the ignition channel, and there are two pressure measurement interfaces in the ignition channel.

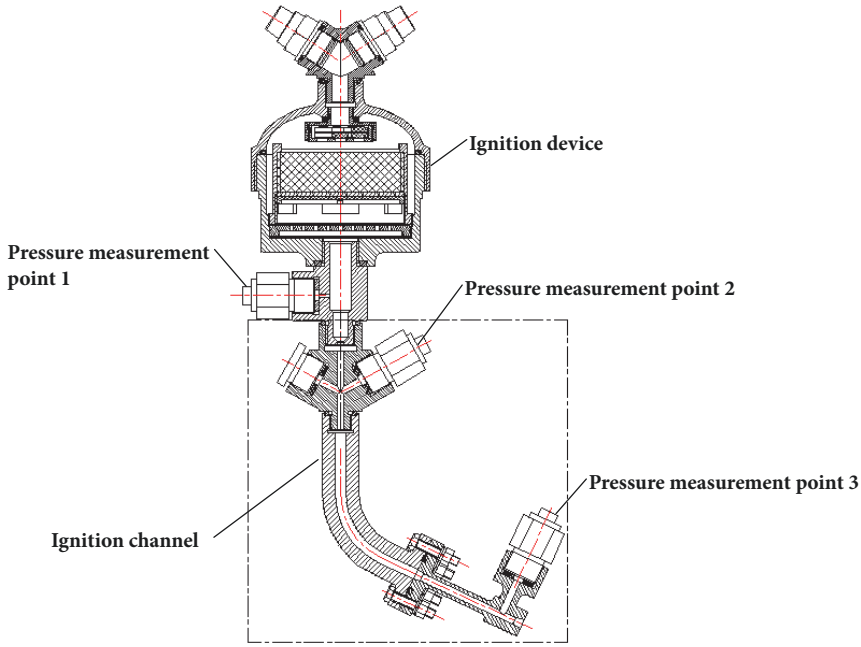

Figure 2: Diagram of the ignition device.

In this study, based on the ignition system of a specific liquid-propellant engine and the ignition channel system in the head of the thrust chamber, ANSYS Fluent software was used to conduct a numerical simulation on the ignition device in two working conditions, namely, with and without the ignition channel. The influences of the two working conditions on the ignition performance of the ignition device, as indicated by the gas pressure, velocity, temperature, flow, and energy, were analyzed. Finally, the results were verified in an experiment. The results of this study provide a basis for the optimal design of the ignition device of liquid-propellant engine.

2. Computation Model

2.1. Model Establishment and Meshing. Figure 2 shows the structure diagram of the ignition device installed on the ignition channel of the liquid-propellant engine. The dashed box is a simplified structure of the ignition channel of the thrust chamber, and outside the dashed box is the main structure of the ignition device, which is connected to the ignition channel in the thrust chamber of the liquid-propellant engine. Moreover, three pressure measurement points were placed at the throat, the four-way valve, and the ignition outlet of the ignition device to measure the pressure during the test.

The diameter, height, and weight of the ignition device are 102mm, 180mm, and 1.5Kg, respectively. In order to adapt to the installation structure of the system, the ignition channel is composed of two straight tubes and a curved section. The diameter of the first straight tube is 4mm, and the length is 45mm. The flow diameter of the curved section is 6mm, and the curvature is 0.021mm^{-1}. There is a long straight tube behind the curved section, with a diameter of 4mm and a length of 75mm. The combustion surface of the solid propellant in the ignition device is fixed, and its burning rate is negatively related to the pressure and is less affected by the pressure change.

According to the given parameters of the ignition device, the physical model was simplified without affecting the analysis results by ignoring the details of chamfering inside the ignition device and the transition at the connection. Models of the internal flow fields under two working conditions (condition I: without ignition channel, condition II: with ignition channel) were created in 3D CAD software, as shown in Figure 3. To simplify the modeling process, only half of a full-scale model was calculated, which was possible due to the geometric symmetry. Meshes were created on the ignition device and inside the ignition channel in ANSYS ICEM CFD—the preprocessing software of Fluent—using tetrahedral unstructured meshes with strong adaptability. Local mesh refinement was carried out in positions with geometric variation like the throat and the ignition channel elbow. Figure 4 shows the meshed internal flow fields in the two working conditions. The total numbers of elements under working conditions I and II are 579,849 and 757,213, respectively.

2.2. Governing Equation. The convective combustion process in the ignition device is very complicated, involving not only the turbulent flow, chemical reaction, and movement of solid particles, but also the strong coupling effect between the flow field and the solid phase. In this study, the physical characteristics of the flow field under stable conditions were analyzed. To facilitate the computation, the following three assumptions were made on the convective combustion process of the ignition device:

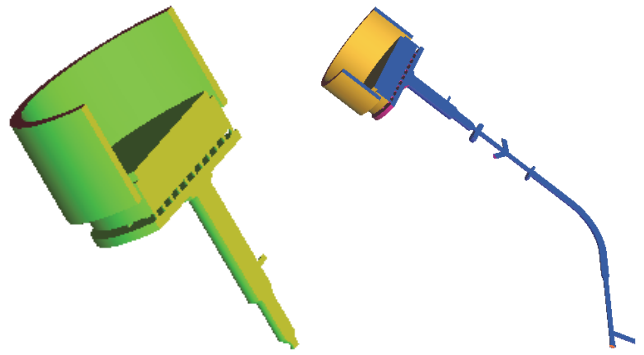

Figure 3: The internal flow fields under working conditions I and II.

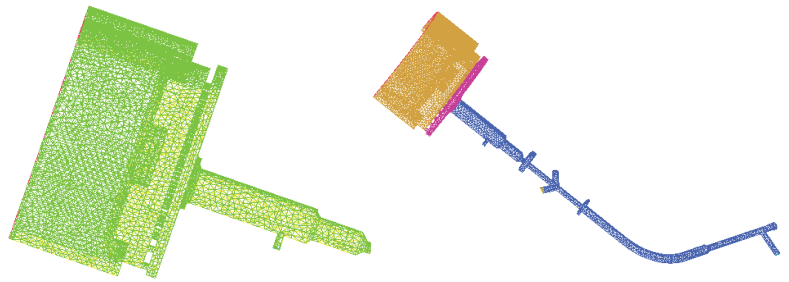

Figure 4: Meshing of the internal flow fields under working conditions I and II.

(1) Both the propellant and gas were in a pure vapor phase stream that followed the law of perfect gas. Therefore, the chemical reaction between the components was ignored and the specific heat capacity at constant pressure was assumed to have stayed constant as the temperature changed.

(2) The influence of erosive burning of the propellant and changes in burning surface were not taken into consideration.

(3) The coupling relationship between the flow field and structure inside the ignition device was not considered.

The flow inside the ignition device is three-dimensional, viscous, and turbulent flow, and its pattern of motion accords with the Navier–Stokes equation of the three-dimensional compressible flow conservation form, which is the nonlinear partial differential control equation to completely describe the turbulent flow. Established based on the law of conservation of fluid mass, momentum, and energy of continuous medium, this equation took into account the impacts of compressibility and viscosity [6]. The conservation form of the differential form of the Reynolds Average N-S control equation in the three-dimensional Cartesian coordinate system is as below: [7]

The mass conservation equation:

$$\frac{\partial \rho}{\partial t} + \frac{\partial}{\partial x_i}\left(\rho u_i\right) = 0 \tag{1}$$

The momentum conservation equation:

$$\frac{\partial \left(\rho u_i\right)}{\partial t} + \frac{\partial}{\partial x_j}\left(\rho u_i u_j\right) + \frac{\partial p}{\partial x_i} = \frac{\partial}{\partial x_j}\tau_{ij} \tag{2}$$

The energy conservation equation:

$$\frac{\partial \left(\rho E\right)}{\partial t} + \frac{\partial}{\partial x_i}\left[\left(\rho E + p\right)u_i\right] = \frac{\partial}{\partial x_i}\left(q_i + u_j \tau_{ij}\right) \tag{3}$$

where ρ, u_i, p, and x_i denote the fluid density, velocity, pressure, and Eulerian coordinate component, respectively; E is the total energy, $E = I + (1/2){u_i}^2$; I denotes internal energy of the gas, $I = C_V T$; q_i is the heat flow, $q_i = \eta(\partial T/\partial x_i)$; and τ_{ij} stands for the shear stress component, $\tau_{ij} = \mu(\partial u_i/\partial x_j + \partial u_j/\partial x_i) - (2/3)\mu\delta_{ij}(\partial u_k/\partial x_k)$. For the equations to be closed, the gas state equation (where R denotes the gas constant) is needed:

$$p = \rho R T. \tag{4}$$

2.3. Turbulent Flow Model. The $k-\varepsilon$ binomial equation with a high computational accuracy was adopted for the turbulent flow model [9].

The k governing equation is

$$\frac{\partial k}{\partial t} + u_i \frac{\partial k}{\partial x_i} = P - \varepsilon + \frac{\partial}{\partial x_i}\left(\frac{\nu_t}{\sigma_k}\frac{\partial k}{\partial x_i}\right). \tag{5}$$

The ε governing equation is

$$\frac{\partial \varepsilon}{\partial t} + u_i \frac{\partial \varepsilon}{\partial x_i} = C_{\varepsilon_1}\frac{\varepsilon}{k}P - C_{\varepsilon_2}\frac{\varepsilon^2}{k} + \frac{\partial}{\partial x_i}\left(\frac{\nu_t}{\sigma_\varepsilon}\frac{\partial \varepsilon}{\partial x_i}\right). \tag{6}$$

Therefore, it could be concluded that

$$\mu_t = \frac{C_\mu k^2}{\varepsilon} \tag{7}$$

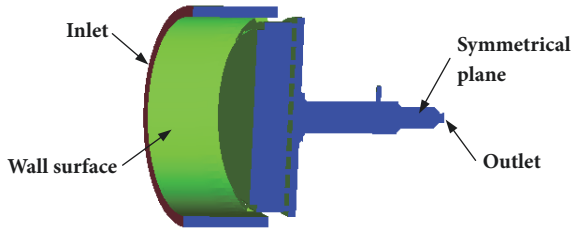

Figure 5: Location of boundary conditions.

where the turbulent flow kinetic energy generation items are $P = 2v_t\overline{S_{ij}}$, $\overline{S_{ij}} = (1/2)(\partial u_i/\partial x_j + \partial u_j/\partial x_i)$, and $v_t = \mu_t/\rho$ and values of the constant terms are $C_\mu = 0.09$, $C_{\varepsilon_1} = 1.44$, $C_{\varepsilon_2} = 1.92$, $\sigma_k = 1.0$, and $\sigma_\varepsilon = 1.3$.

2.4. Initial and Boundary Conditions. The boundary conditions in this study were set up for the inlet, wall surface, and symmetrical plane of the internal flow field of the ignition device and the ignition outlet, as shown in Figure 5. The initial conditions, boundary conditions, and working medium were defined as below.

(1) Initial Conditions. The initial conditions started when the main powder loaded in the ignition device was ignited, and at this time, the pressure and temperature inside the ignition device were consistent with the atmospheric pressure and temperature; that is, $P = 0.101$MPa and $T = 298$K; at this time, the three components of velocity (the turbulent kinetic energy, turbulence momentum, and heat dissipation rate) were all assigned relatively small values, namely, $u_i(0, x, y, z) = 0.01m/s$, $k = 1$, and $\varepsilon = 1$. [9]

(2) Boundary Conditions of the Inlet. Pressure inlet boundary condition was used for the inlet of the internal flow field of the ignition device. The average temperature at the inlet is the gas temperature $T = 1950.4$K and the average pressure at the inlet $P = 8$MPa.

(3) Boundary Conditions of the Wall Surface. As the average temperature at the inlet had considered the heat loss, the adiabatic wall surface was applied; that is, the gradients of speed, temperature, and pressure were all zero.

(4) Symmetrical Boundary Conditions. Since the internal flow field of the ignition device was symmetrical, half of the flow was calculated. The pressure, density, temperature, and velocity gradient on the symmetrical boundary were zero.

(5) Boundary Conditions of the Ignition Outlet. Pressure outlet boundary condition was used for the ignition outlet of the ignition device. The average pressure at the outlet was based on the standard atmospheric pressure $P = 0.101$MPa; the average temperature was $T = 298$K.

(6) Working Medium. High-temperature gas was the working medium in the internal flow field of the ignition device. Without considering two-phase flow, the gas was in the pure gas phase. Equivalent to a single ideal gas with certain thermodynamic properties, the ideal gas was used in the simulation carried out in this study. The gas temperature $T = 1950.4$K, the dynamic viscosity of the gas $\mu_g = 1.789 \times 10^{-5}\text{kg} \cdot \text{m}^{-1} \cdot s^{-1}$, the heat conductivity coefficient of the gas $\lambda_g = 0.0242\text{W} \cdot \text{m}^{-1} \cdot K^{-1}$, the specific heat capacity of the gas $c_p = 1651J \cdot \text{kg}^{-1} \cdot K^{-1}$, and the molar mass fraction of the gas $M = 24.71\text{kg} \cdot \text{mol}^{-1}$.

3. Simulation Results and Analysis

As gas pressure, velocity, temperature, flow rate, and energy are important indexes to characterize the working performance of the ignition device, a steady-state computation was carried out on relevant parameters of the flow fields of the ignition channels of the ignition device under working conditions I and II, respectively. The influences of the ignition channel on the working process of the ignition device were analyzed by comparing the results obtained.

3.1. Influence of Ignition Channel on Gas Pressure. As shown in Figure 6(a), under working condition I, the gas pressure gradually decreased from the convergent section to the expanding section and reached the lowest value (2.24 MPa) at the ignition outlet.

Under working condition II (as shown in Figure 6(b)), the gas pressure at the throat was 13.5% higher than that under working condition I. Subsequently, the gas pressure was reduced by 16% due to resistance when the gas flowed through the straight tube in the back part of the throat. In the curved section after the straight tube, as the gas velocity declined rapidly, the gas pressure rose according to the Bernoulli effect (as shown in Figures 6(c) and 6(d), the gas velocity declined after entering the curved section, and the gas pressure rose accordingly). There was a long straight tube behind the curved section, and as its cross section area became smaller, the gas velocity gradually increased due to the convergence of the cross section, and the corresponding gas pressure gradually decreased. As the cross section expanded at the outlet of the ignition channel, the gas expanded and accelerated and the gas pressure drastically reduced, reaching the lowest value (0.91 MPa) at the ignition outlet, which was 60% lower than that under working condition I, yet still higher than the atmospheric pressure, so the initial ignition would not be affected.

During the whole working process from ignition to stable combustion, the pressure in the main combustion chamber of the thrust chamber of liquid-propellant engine will increase from the atmospheric pressure to the working pressure, and the ignition device must work continuously to maintain ignition stability. The gas pressure at the ignition outlet under working conditions I and II was analyzed during the process when the pressure in the main combustion chamber of the thrust chamber rose from the atmospheric pressure (0.1 MPa) to the working pressure (6 MPa); the results are shown in Figure 7, where Pa means the pressure in the main combustion chamber and Pe means the pressure at the ignition outlet.

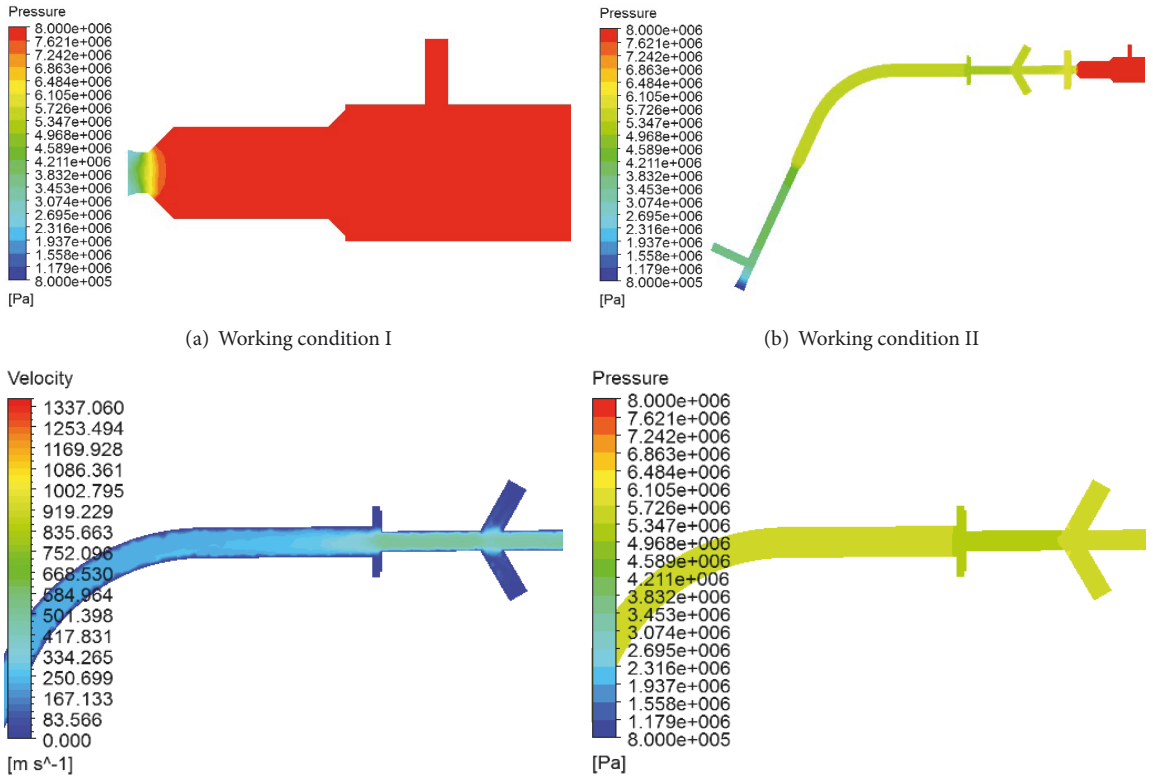

(a) Working condition I

(b) Working condition II

(c) Velocity of the curved section

(d) Pressure of the curved section

Figure 6: Static pressure nephograms of the symmetrical planes of the internal flow fields in two working conditions and the Bernoulli effect of the curved section.

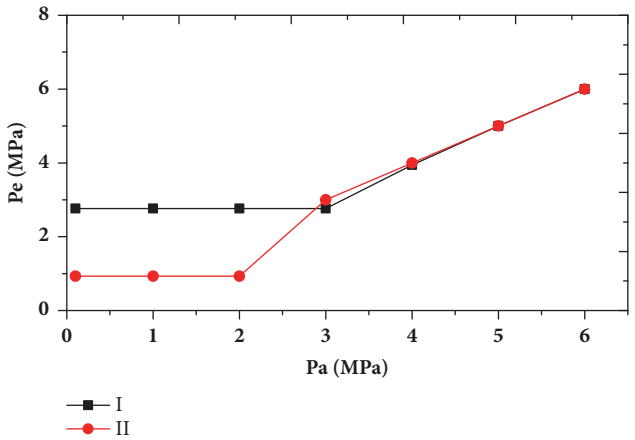

Figure 7: Variation of gas pressure at the ignition outlet with the pressure in the main combustion chamber.

As shown in Figure 7, when the pressure in the main combustion chamber was equal to the atmospheric pressure, the gas pressure at the ignition outlet under working condition II was lower than that under working condition I. As the pressure in the main combustion chamber increased, the gas pressures at the ignition outlet under the two working conditions were first in a stable state and then increased rapidly after a certain critical value.

Under working condition I, when the pressure in the main combustion chamber varied from 0 to 3 MPa, the gas pressure at the ignition outlet remained constant, and after the pressure in the main combustion chamber increased to 3 MPa, the gas pressure at the ignition outlet rose synchronously; under working condition II, as the pressure in the main combustion chamber varied from 0 to 2 MPa, the gas pressure at the ignition outlet remained unchanged, and after the pressure in the main combustion chamber increased to 2 MPa, the gas pressure at the ignition outlet went up synchronously.

Based on the gas pressure nephograms influenced by pressure variation in the main combustion chamber under working condition II (Figure 8), the specific reason for the presence of a critical value was obtained, where critical value means the pressure value corresponding to the disturbed region which occurs at the ignition outlet. When the pressure in the main combustion chamber is larger than the gas pressure at the ignition outlet, the jet flow jetted at the ignition outlet was compressed by pressure in the main combustion chamber, causing disturbed region (as shown in Figure 8(b)) and affecting the flow at the ignition outlet. As the pressure in the main combustion chamber gradually increased, the disturbed region moved towards the upstream of the ignition outlet (as shown in Figures 8(c) and 8(d)), causing the gas pressure at the ignition outlet to rise simultaneously with the pressure in the main combustion chamber.

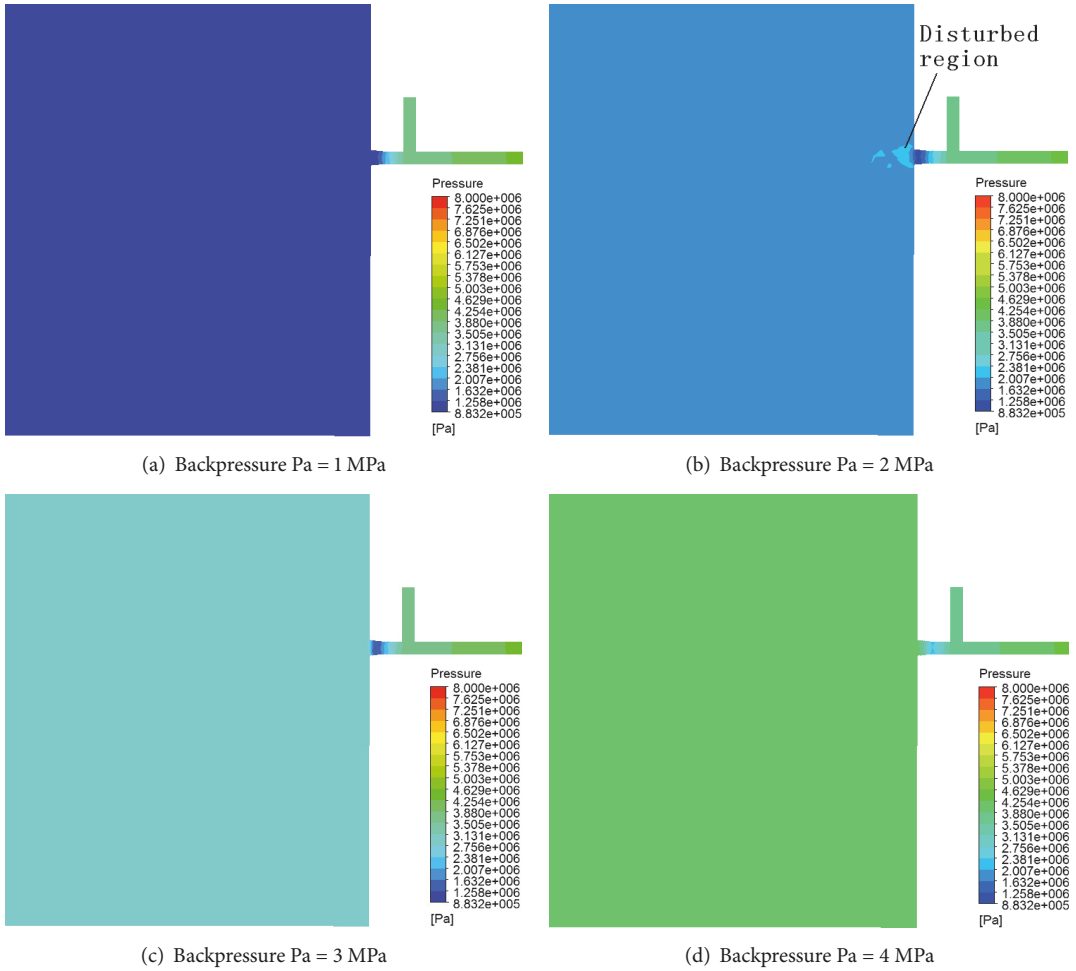

(a) Backpressure Pa = 1 MPa (b) Backpressure Pa = 2 MPa

(c) Backpressure Pa = 3 MPa (d) Backpressure Pa = 4 MPa

Figure 8: Variation of the gas pressure nephogram under working condition II with the pressure in the main combustion chamber.

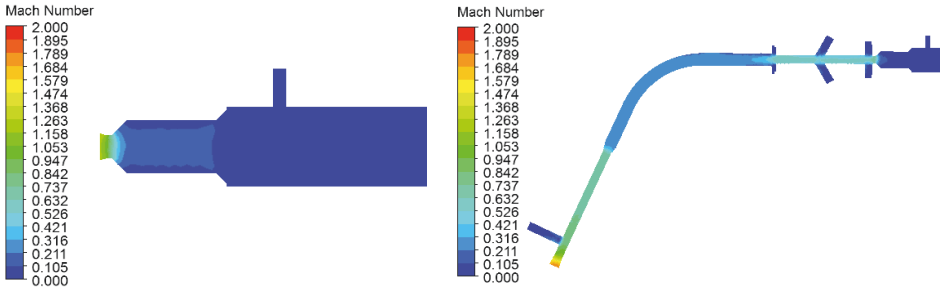

(a) Working condition I (b) Working condition II

Figure 9: Mach number nephograms of the symmetrical planes of the internal flow fields in the two working conditions.

3.2. Influence of Ignition Channel on Gas Velocity. As shown in Figure 9, under working condition I, with the gradual decrease of the cross section area, the gas velocity in the convergent section in the front of the throat increased gradually from the subsonic velocity to the sonic velocity and finally reached 1 Ma at the throat. As the cross section area gradually increased, the gas continued to expand and accelerate in the divergent section behind the throat and finally reached a maximum of 1.27 Ma at the ignition outlet. Overall, the whole flow was in accordance with the characteristics of nozzle flow.

Under working condition II, since the ignition channel was placed behind the ignition device, the gas velocity at the throat of the ignition device did not reach the sonic speed and its value was about 0.5 Ma under the influence of the flow resistance of the ignition channel. There was a small section of straight tube in the back part of the throat whose cross section

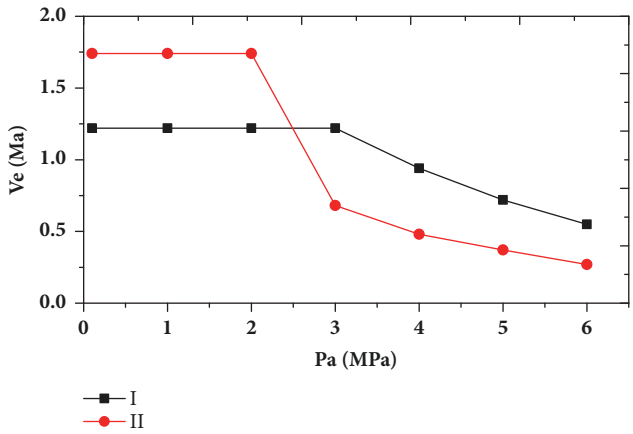

Figure 10: Variation of gas velocity at the ignition outlet with the pressure in the main combustion chamber.

area remained constant and the gas speed remained basically unchanged. There was a relatively long curved section in the ignition channel behind the straight tube where the local flow resistance of gas increased and the cross section diameter increased by 50% compared to the straight tube, and the gas speed decreased to 0.23 Ma after it flowed through this section. There was a comparatively long straight tube behind the curved section in which the cross section area became smaller and the gas velocity increased gradually from a subsonic to sonic speed under the convergence of the cross section. As the cross section expanded at the ignition outlet, the gas continued to expand and accelerate, and its speed reached a maximum of 1.78 Ma at the ignition outlet, which was 40% higher than that under working condition I, and which would be conducive to the initial ignition.

Figure 10 shows the analysis results about the gas velocity at the ignition outlet under working conditions I and II as the pressure in the main combustion chamber of the thrust chamber increased from the atmospheric pressure (0.1 MPa) to the working pressure (6 MPa), where Ve means the gas velocity at the ignition outlet.

It can be seen from Figure 10 that when the pressure in the main combustion chamber was equal to the atmospheric pressure, the gas velocity at the ignition outlet under working condition II was higher than that under working condition I, and as the pressure in the main combustion chamber increased, the gas velocity in both of the working conditions was first in a stable state and then declined rapidly.

According to the analysis conducted in Section 3.1, when the pressure in the main combustion chamber is smaller than the critical value, the supersonic airflow has no effect on the gas flow at the ignition outlet, and the gas speed at the ignition outlet remains unchanged. When the main combustion chamber pressure increases to the critical value, the disturbed region appears at the ignition outlet. Because the gas velocity in the ignition outlet is supersonic flow (1.75 Ma), shock waves will occur in the disturbed region, and the velocity of supersonic flow becomes subsonic flow through shock wave. When the pressure in the main combustion chamber exceeded the critical value, as the shock waves at the ignition outlet move upstream of the outlet, the gas pressure at the ignition outlet begins to increase gradually as the pressure in the main combustion chamber rises, yet its flow velocity continues to decrease.

In the case of working condition I, when the pressure in the main combustion chamber varied from 0 to 3 MPa, the gas velocity at the ignition outlet remained constant and it decreased after the pressure in the main combustion chamber increased to 3 MPa. Under working condition II, when the pressure in the main combustion chamber varied from 0 to 2 MPa, the gas velocity at the ignition outlet remained constant and it declined rapidly as the pressure in the main combustion chamber increased to 2 MPa, and the final gas velocity at the ignition outlet was smaller than that under working condition I, which would adversely affect the ignition. Figure 11 shows variation of the gas velocity nephogram under working condition II as the pressure in the main combustion chamber changed.

3.3. Influence of Ignition Channel on Gas Temperature. As shown in Figure 12, under working condition I, the gas temperature gradually dropped from the convergent section to the divergent section of the throat and reached the lowest value (1,628 K) at the ignition outlet. In the case of working condition II, the gas temperature at the throat of the ignition device was 3.7% higher than that under working condition I, and it decreased by 2.4% due to resistance when the gas flowed through the straight tube in the back part of the throat. In the curved section following the straight tube, since the gas pressure increased, the gas temperature increased synchronously and the temperature rise rate was smaller than the pressure rise rate according to the principle that $T^k/P^{(k-1)}$ is constant during the heat insulation process (where T denotes the gas temperature, P is the gas temperature, and k stands for the gas adiabatic exponent). In the long straight tube behind the curved section, the gas flow gradually increased due to the convergence of the cross section, and the gas pressure gradually declined while the gas temperature gradually increased. Due to gas expansion and acceleration, the gas pressure at the ignition outlet dropped drastically, and the gas temperature also drastically reduced to 1,386 K at the ignition outlet, which was 15% lower than that under working condition I. However, the temperature at the ignition outlet was still high enough to have little effect on the initial ignition.

Figure 13 shows the analysis results about the gas temperature at the ignition outlet under working conditions I and II as the pressure in the main combustion chamber increased from the atmospheric pressure (0.1 MPa) to the working pressure (6 MPa), where Te means the gas temperature at the ignition outlet.

As shown in Figure 13, there was a slight difference in the gas temperature at the ignition outlet under working conditions I and II, indicating that the gas temperature would have no quantifiable influence on the ignition process under the two working conditions. With the increase of pressure in the main combustion chamber, the gas temperature under both conditions was initially in a stable state and then gradually increased; the gas flow at the ignition outlet was

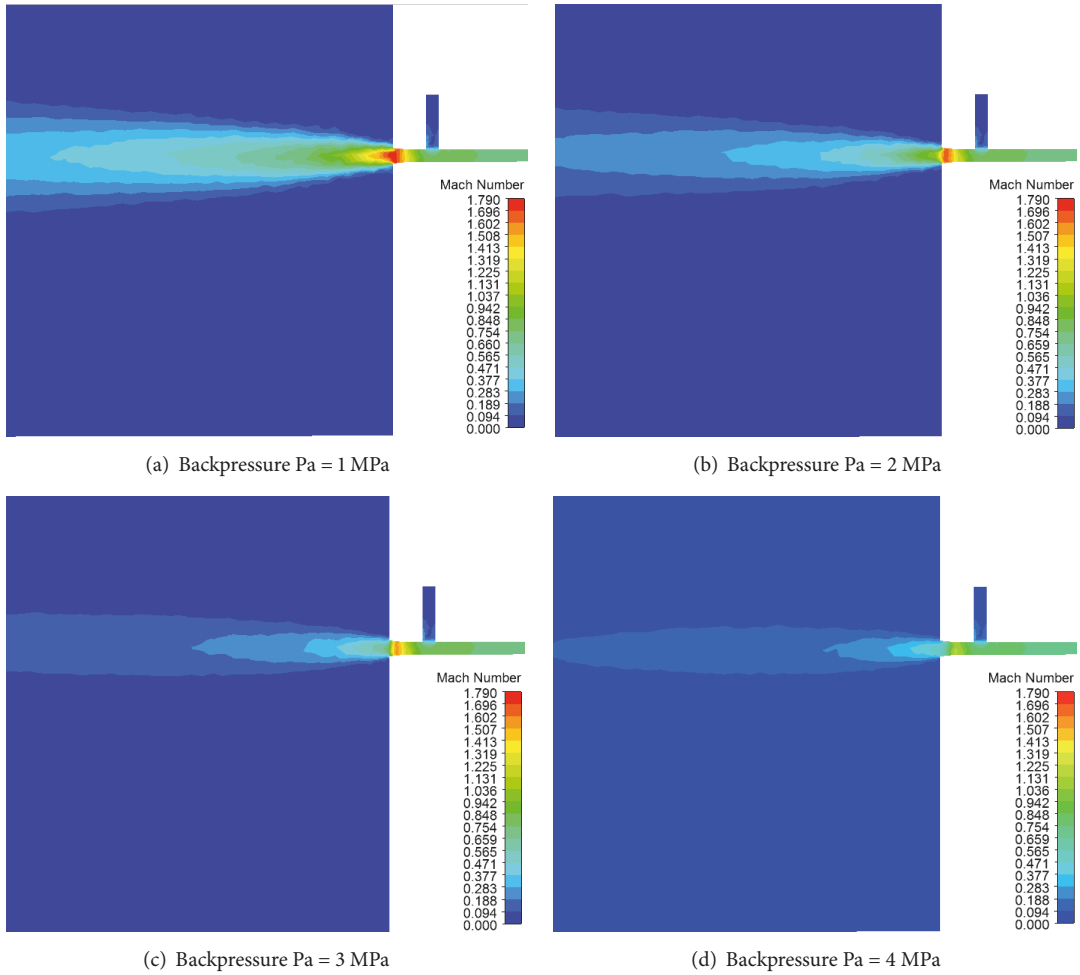

(a) Backpressure Pa = 1 MPa

(b) Backpressure Pa = 2 MPa

(c) Backpressure Pa = 3 MPa

(d) Backpressure Pa = 4 MPa

Figure 11: Variation of the gas velocity nephogram under working condition II with the pressure in the main combustion chamber.

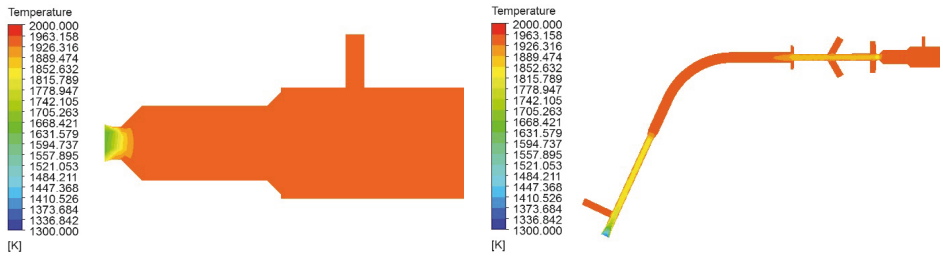

(a) Working condition I

(b) Working condition II

Figure 12: Static temperature nephograms of the symmetrical planes of the internal flow fields in the two working conditions.

affected when the pressure in the main combustion chamber increased to a critical value; and as the pressure in the main combustion chamber increased, the gas temperature at the ignition outlet rose simultaneously and the gas temperature increased gradually. For working condition I, the gas temperature at the ignition outlet remained constant as the pressure in the main combustion chamber varied from 0 to 3 MPa, yet as it increased to 3 MPa, the gas pressure at the ignition outlet rose synchronously and the corresponding gas temperature increased gradually with the increase of pressure in the main combustion chamber. Under working condition II, the gas temperature at the ignition outlet remained constant as the pressure in the main combustion chamber varied from 0 to 2 MPa, yet after it increased to 2 MPa, the gas pressure at the ignition outlet began to increase synchronously and the corresponding gas temperature rose gradually as the pressure in the main combustion chamber increased. Figure 14 shows variation of the gas temperature nephogram under working

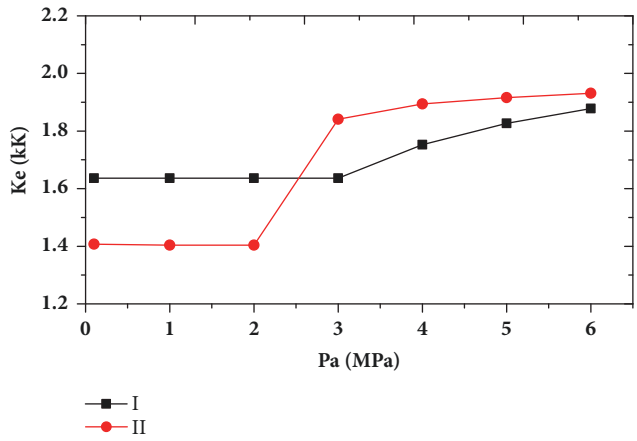

Figure 13: Variation of gas temperature at the ignition outlet with the pressure in the main combustion chamber.

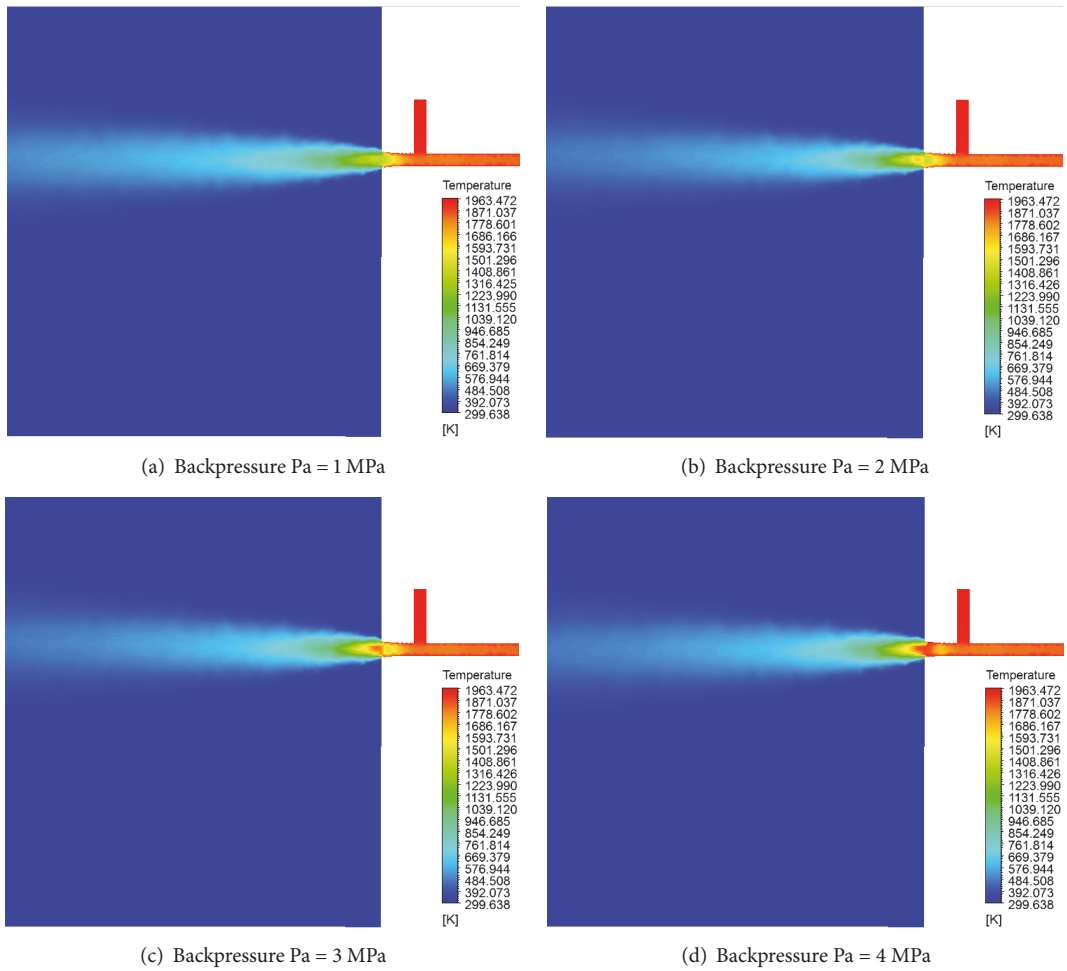

(a) Backpressure Pa = 1 MPa

(b) Backpressure Pa = 2 MPa

(c) Backpressure Pa = 3 MPa

(d) Backpressure Pa = 4 MPa

Figure 14: Variation of the gas temperature nephogram under working condition II with the pressure in the main combustion chamber.

condition II as the pressure in the main combustion chamber changed.

3.4. Influence of Ignition Channel on Gas Flow. Figure 15 shows the analysis results about the gas flow under working conditions I and II as the pressure in the main combustion chamber of the thrust chamber rose from the atmospheric pressure (0.1 MPa) to the working pressure (6 MPa). As shown in the figure, the gas flow under working condition II was 12.7% lower than that under working condition I, which will not have a significant influence on the ignition process because of little difference in gas flow. With the increase

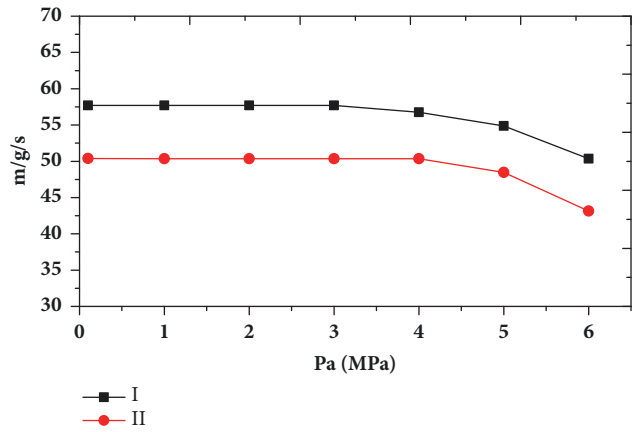

Figure 15: Variation of gas flow with the pressure in the main combustion chamber.

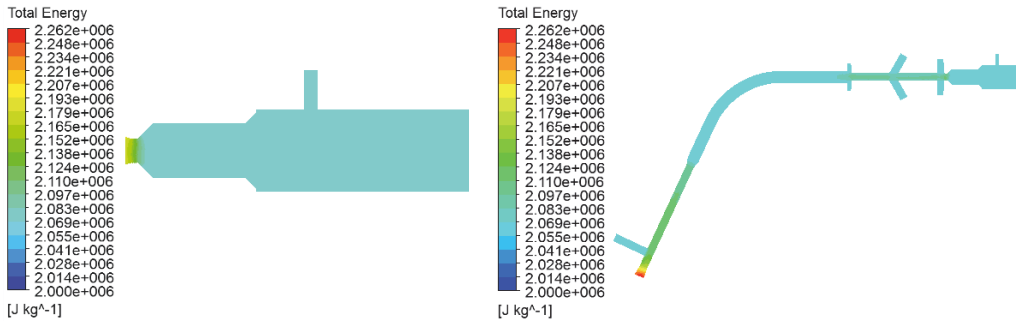

(a) Working condition I (b) Working condition II

Figure 16: Energy nephograms of the symmetrical planes of the internal flow fields in the two working conditions.

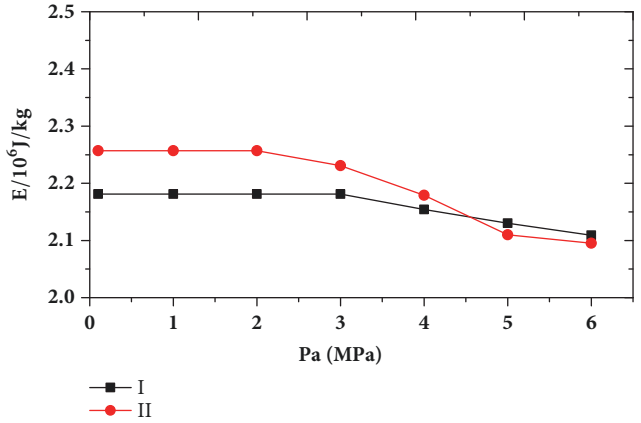

Figure 17: Variation of gas energy at the ignition outlet with the pressure in the main combustion chamber.

of the pressure in the main combustion chamber, gas flow in both conditions was initially in a stable state and then gradually decreased, yet the overall variation was not large, so the ignition process would not be significantly influenced by gas flow.

3.5. Influence of Ignition Channel on Gas Energy. From Figure 16, it can be seen that the total gas energy at the ignition outlet was 2.18×10^6 J/kg under working condition I and 2.26×10^6 J/kg under working condition II, which is 3.7% higher, indicating that there is slight difference between the two conditions.

Figure 17 shows the analysis results for variation of gas energy at the ignition outlet under working conditions I and II as the pressure in the main combustion chamber rose from the atmospheric pressure (0.1 MPa) to the working pressure (6 MPa). As shown in Figure 17, as the pressure in the main combustion chamber increased, the gas energy

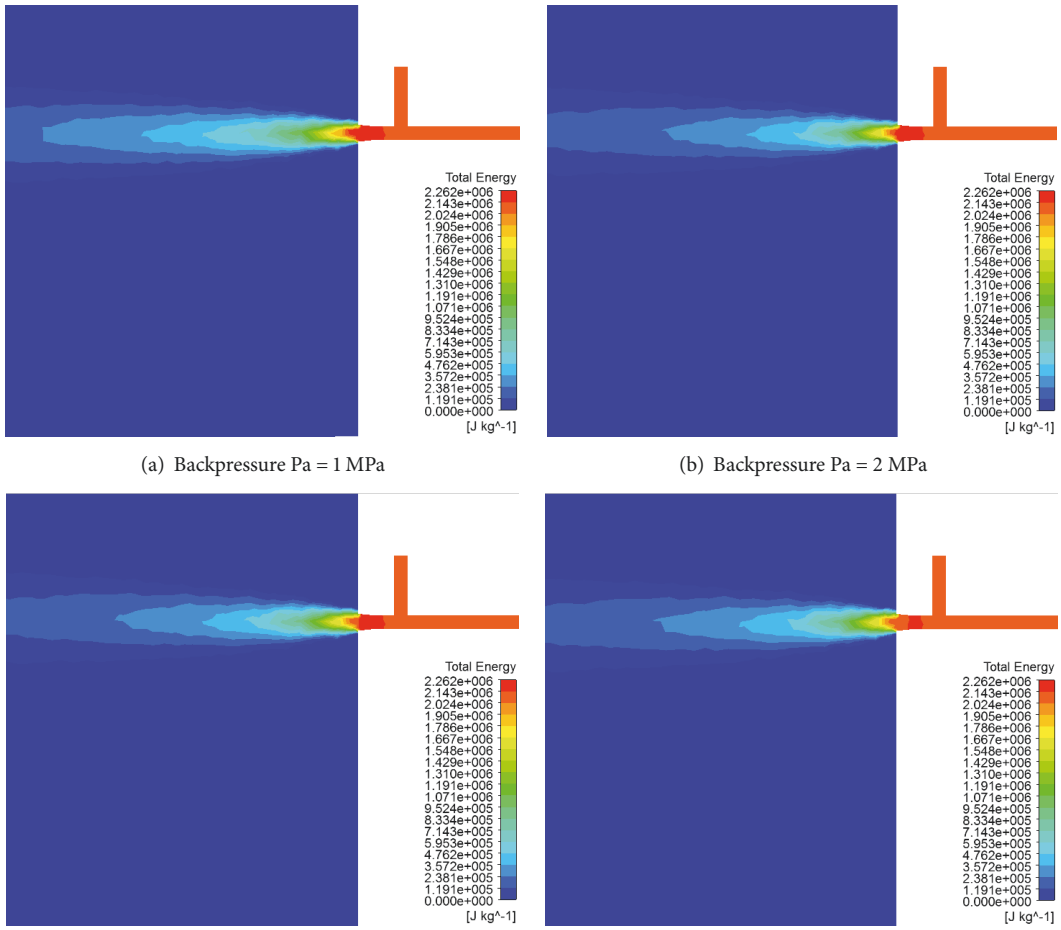

(a) Backpressure Pa = 1 MPa

(b) Backpressure Pa = 2 MPa

(c) Backpressure Pa = 3 MPa

(d) Backpressure Pa = 4 MPa

Figure 18: Variation of the gas energy nephogram under working condition II with the pressure in the main combustion chamber.

at the ignition outlet under both workings conditions was initially in a steady state and then gradually decreased. This occurred because when the pressure in the main combustion chamber increased to the critical value, the gas flow at the ignition began to be affected and the total gas energy E was synchronously influenced. $E = I + (1/2)u_i^2$, where I denotes the internal energy of the gas which is related to the gas flow and u_i stands for the gas velocity. According to the analysis results in Sections 3.2 and 3.4, both the gas flow and gas velocity at the ignition outlet were characterized by a declining trend after reaching a critical value, and therefore the total gas energy decreased synchronously.

Under working condition I, when the pressure in the main combustion chamber varied from 0 to 3 MPa, the gas energy at the ignition outlet remained constant, yet as the pressure increased to 3 MPa, the gas energy gradually decreased with the increase of the pressure in the main combustion chamber. For working condition II, when the pressure in the main combustion chamber changed from 0 to 2 MPa, the gas energy at the ignition outlet remained constant, yet as the pressure increased to 2 MPa, the gas energy gradually decreased as the pressure in the main combustion chamber increased. Since there was no significant change in terms of the gas energy, gas energy would not have a significant impact on the ignition process under the two working conditions. Figure 18 shows variation of the gas energy nephogram under working condition II as the pressure in the main combustion chamber changed.

4. Experimental Verification

To verify the reliability of the numerical model and the computation method, an experimental test was performed on the ignition device under working conditions I and II, where atmospheric pressure was used as the backpressure at the ignition outlet. Considering that the combustion temperature (1950.4 K) is the intrinsic characteristic of the main powder loaded in the ignition device, there is historical test data on this topic, and the gas temperature does not change substantially; no further measurement was performed in this study. As it was difficult to accurately measure the gas velocity and gas energy during the test, the gas pressure at each position was measured during the test and then converted into the gas flow according to the working time of the ignition device. Under working condition I, the gas pressure at the throat of the ignition device was measured, as shown in

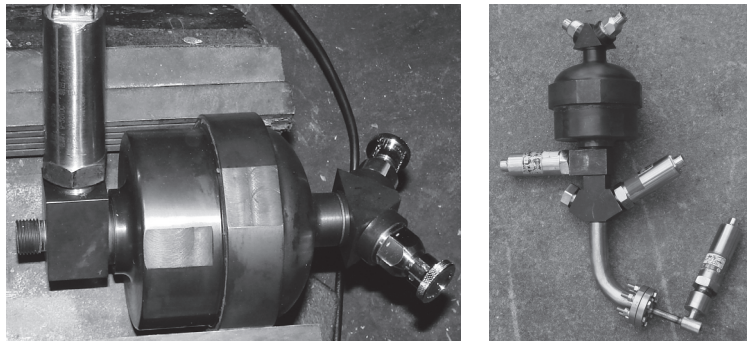

(a) Working condition I (b) Working condition II

Figure 19: Test of the ignition device in two working conditions.

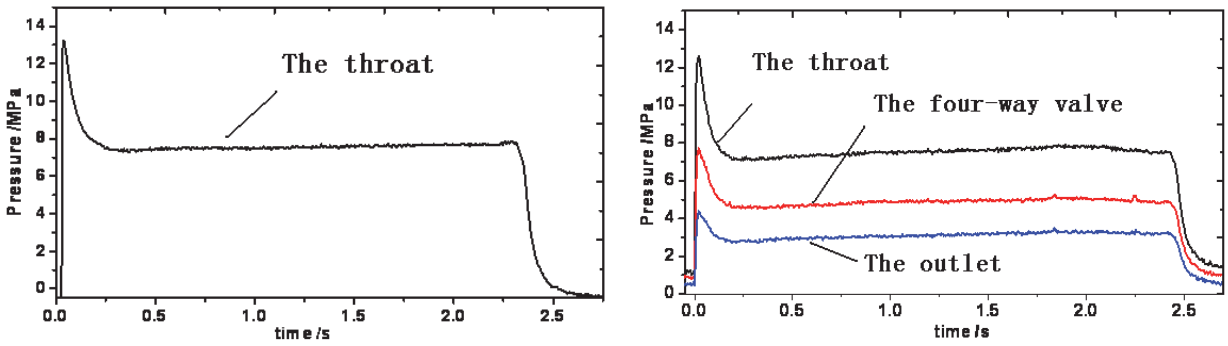

(a) Working condition I (b) Working condition II

Figure 20: Pressure-time curves measured in two working conditions.

Figure 19(a). In the case of working condition II, the gas pressure was measured at the throat of the ignition device, the first section of straight tube of the ignition channel, and the outlet of the ignition channel, as shown in Figure 19(b). Figure 20 shows the pressure-time curves measured in the two working conditions by the pressure transmitter and the multichannel data acquisition system.

As indicated by Figure 20, under working condition I, the working pressure at the throat of the ignition device was 7.8 MPa, and the working time was 2.32 s (when the pressure rises to more than 0.3 MPa as the starting point, the intersection point of the curve work section and the descending section is the end point of the work time), which was converted into a mass flow rate of 53g/s; under working condition II, the working pressure at the throat of the ignition device was 7.52 MPa, the pressure in front of the ignition channel outlet was 3.38 MPa, and the working time was 2.4 s, which was converted into a mass flow rate of 50.79 g/s.

The numerical computation results at each measurement point obtained by ANSYS Fluent and the test results were compared, as shown in Table 1.

From Table 1, it can be seen that the simulation results were close to the test results, which indicated that the numerical model and computation methods are effective, and the analysis results can guide parameter design of the ignition device.

5. Discussion and Conclusions

Based on different working performances of the ignition device of the liquid-propellant rocket engine under two working conditions (condition I: without ignition channel, condition II: with ignition channel), ANSYS Fluent flow field computation software was used to conduct a numerical simulation of the steady flow field in the two working conditions. The results were analyzed to determine the variations of important indexes that influence the working performance of the ignition device, such as the gas pressure, velocity, temperature, flow, and energy. The following conclusions were obtained:

(1) The gas pressure at the throat of the ignition device was 13.5% higher with the ignition channel (condition II) than without the ignition channel (condition I), so the structural strength of the throat should be calculated and evaluated. The gas pressure at the ignition outlet was 60% lower under condition II compared to condition I, yet it was still higher than the atmospheric pressure, so it would not affect the initial ignition. As the pressure in the main combustion chamber gradually increased to 2 MPa in the ignition process (condition II), the gas pressure at the ignition outlet experienced an inflection point and began to rise.

(2) With the ignition channel (condition II), the gas velocity at the throat of the ignition device did not reach

Table 1: Test and simulation results.

Results	Working condition					
	Working condition I		Working condition II			
	Pressure at the throat (MPa)	Mass flow rate (g/s)	Pressure at the throat (MPa)	Pressure of the straight tube in the first section (MPa)	Pressure at the outlet (MPa)	Mass flow rate (g/s)
Simulation results	7.96	57.71	7.98	5.64	3.71	50.4
Experiment results	7.8	53	7.52	5.3	3.38	50.79
Deviation (%)	−2	−8.6	−5.76	−6.03	−8.89	+0.7

sonic speed, the position of sonic velocity moved to the downstream section of the ignition channel, and the gas velocity at the ignition outlet was 40% higher than under condition I. However, as the pressure in the main combustion chamber increased to 2 MPa during the ignition process, the gas velocity at the ignition outlet experienced an inflection point and began to decline rapidly. A low gas velocity at the ignition outlet would adversely affect the ignition. Therefore, to improve the ignition reliability, the combustion pressure of the ignition device needs to be changed so as to increase the inflection point value of the pressure in the combustion chamber when the gas velocity at the ignition outlet decreases.

(3) Under the influence of the ignition channel (condition II), the gas temperature at the throat of the ignition device and the ignition outlet was not greatly different from the temperature in the corresponding positions under the condition without the ignition channel (condition I), and it was not significantly affected by variation of the pressure in the main combustion chamber. Therefore, gas temperature does not have a significant influence on the ignition process.

(4) Under the working condition with the ignition channel (condition II), the gas flow at the ignition outlet was 12.7% smaller than without the ignition channel (condition I), which would not have an obvious effect on the ignition process. As the pressure in the main combustion chamber gradually increased, the gas flow at the ignition outlet gradually decreased, yet the overall variation was not obvious. Therefore, the ignition process is not significantly influenced by gas flow.

(5) Under the influence of the ignition channel (condition II), the gas energy at the ignition outlet was 3.7% higher than that under the working condition with no ignition channel (condition I). Higher gas energy at the ignition outlet is favorable to the initial ignition, yet the difference in energy observed between conditions I and II was not significant. With the gradual increase of the pressure in the main combustion chamber, the gas energy at the ignition outlet gradually decreased, yet the overall change was not apparent. Therefore, using an ignition channel does not affect gas energy to an extent that would have a significant influence on the ignition process.

This paper analyzes the difference in the ignition performance of the ignition device under the conditions of without ignition channel and with ignition channel, which can provide references for similar problems. Based on this research, in future work, the study should optimize the ignition channel's structural parameters, such as the diameter of the channel, the length of the channel, and the curvature of the curved section, so as to improve the ignition performance and get the optimal design results.

Conflicts of Interest

The authors declare that they have no conflicts of interest.

References

[1] P. Baudart, V. Duthoit, and J. Harlay, "Numerical simulation of cryotechnic rocket engine ignition," in *Proceedings of the 27th Joint Propulsion Conference*, Sacramento,CA,U.S.A..

[2] R. Buttay, L. Gomet, G. Lehnasch, and A. Mura, "Highly resolved numerical simulation of combustion downstream of a rocket engine igniter," *Shock Waves*, vol. 27, no. 4, pp. 655–674, 2017.

[3] M. POPP and J. Stanke, "Experimental investigation of the HM7B thrust chamber start-up transient," in *Proceedings of the 24th Joint Propulsion Conference*, Boston,MA,U.S.A..

[4] L. d'Agostino, L. Biagioni, and G. Lambert, "An ignition transient model for solid propellant rocket motors," in *Proceedings of the 37th Joint Propulsion Conference and Exhibit 2001*, usa, July 2001.

[5] C. Bo, L. Mu, W. Bao-yuan et al., "Numerical study on igniter performance of liquid ramjet combustor," *Journal of rocket Propulsion*, vol. 39, no. 6, pp. 6–11, 2013.

[6] Y. Le, Y. Zhen-yong, and H. Jing-xuan, "A FLUENT analysis of influencing factors for SRM inner flow field simulation at ignition," *Journal of Solid Rocket Technology*, vol. 34, no. 4, pp. 474–477, 2011.

[7] Y. Le, Y. Zhen-yong, and H. Jing-xuan, "Calculation Model of Inner Flow Field of Solid Rocket Motor in Ignition Transient," *Missiles and Space vehicles*, no. 6, pp. 75–77, 2015.

[8] B.-S. Tang, J. Chen, F. Feng, J. Cao, and H.-C. Li, "Numerical simulation of diaphragm rupture process of igniter in ignition process of solid rocket motor," *Guti Huojian Jishu/Journal of Solid Rocket Technology*, vol. 36, no. 6, pp. 753–757, 2013.

[9] X. Xue-wen, M. Jun-lin, R. Jian-cun et al., "The analyses of transient flow-field characteristics in nozzle of SRM," *Journal of Rocket Propulsion*, vol. 41, no. 5, pp. 49–53, 2015.